

# Redistributing the Precision and Content in 3D-LUT-based Inverse Tone-mapping for HDR/WCG Display

Cheng Guo

State Key Laboratory of Media  
Convergence and Communication,  
Communication University of China  
guocheng@cuc.edu.cn

Leidong Fan

School of Electronic and Computer  
Engineering, Shenzhen Graduate  
School, Peking University  
fanleidong@stu.pku.edu.cn

Qian Zhang

Academy of Broadcasting Planning  
Beijing, China  
zhangfanqian@139.com

Hanyuan Liu

Academy of Broadcasting Planning  
Beijing, China  
lhy2871@126.com

Kanglin Liu

Peng Cheng Laboratory  
Shenzhen, China  
max.liu.426@gmail.com

Xiuhua Jiang

Peng Cheng Laboratory  
Shenzhen, China  
jiangxiuhua@cuc.edu.cn

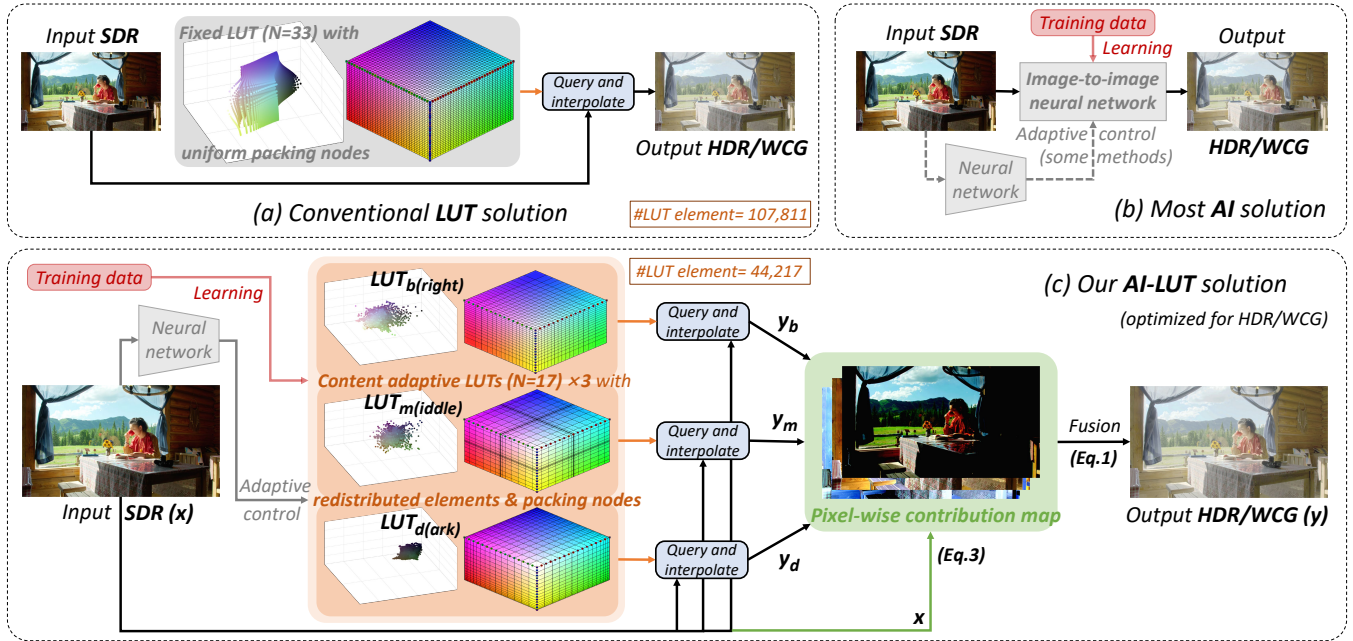


**Figure 1: Different ITM (inverse tone-mapping) solutions.** Conventional LUT (a) lacks adaptability. While for user-end application, end-to-end AI methods (b) fail for efficiency. Therefore, we combine AI with LUT: our LUT is learned from training data, and varies with input ( $x$ ). Also, we use 3 smaller LUTs ( $N=17$ ) with explicitly-defined non-uniform packing precision (colored cube) respectively denser in dark, middle and bright range. Then, a pixel-wise contribution map is used to combine the best part of 3 results ( $y_b$ ,  $y_m$  and  $y_d$ ), and the output content of 3 LUTs (colored dots) will also be redistributed during learning. In this case, we reach similar performance to single bigger LUT ( $N=33$ ), yet occupying fewer #param of LUT ( $44217 < 107811$ ).

## ABSTRACT

ITM (inverse tone-mapping) converts SDR (standard dynamic range) footage to HDR/WCG (high dynamic range /wide color gamut) for media production. It happens not only when remastering legacy SDR footage in front-end content provider, but also adapting on-the-air SDR service on user-end HDR display. The latter requires more efficiency, thus the pre-calculated LUT (look-up table) has become a popular solution. Yet, conventional fixed LUT lacks adaptability, so we learn from research community and combine it with AI. Meanwhile, higher-bit-depth HDR/WCG requires larger LUT than

SDR, so we consult traditional ITM for an efficiency-performance trade-off: We use 3 smaller LUTs, each has a non-uniform packing (*precision*) respectively denser in dark, middle and bright luma range. In this case, their results will have less error only in their own range, so we use a contribution map to combine their best parts to final result. With the guidance of this map, the elements (*content*) of 3 LUTs will also be redistributed during training. We conduct ablation studies to verify method's effectiveness, and subjective and objective experiments to show its practicability. Code is available at: <https://github.com/AndreGuo/ITMLUT>.

## CCS CONCEPTS

• **Applied computing** → **Media arts**; • **Computing methodologies** → **Image processing**; **Computational photography**.

## KEYWORDS

Look-up Table, Inverse Tone-mapping, High Dynamic Range, Wide Color Gamut, Deep Learning

### ACM Reference Format:

Cheng Guo, Leidong Fan, Qian Zhang, Hanyuan Liu, Kanglin Liu, and Xihua Jiang. 2023. Redistributing the Precision and Content in 3D-LUT-based Inverse Tone-mapping for HDR/WCG Display. In *European Conference on Visual Media Production (CVMP '23)*, November 30-December 1, 2023, London, United Kingdom. ACM, New York, NY, USA, 10 pages. <https://doi.org/10.1145/3626495.3626503>

## 1 INTRODUCTION

In media industry, ultra-high definition (UHD) surpasses high-definition (HD) in 5 dimensions: resolution, frame-rate, bit-depth, dynamic range and color gamut. The first 3 belong to *definition* which gives a more precise description, while the last 2 bring advances in *expressiveness* via larger luminance and color container: Image/video with  $>1000\text{nit}$  max-luminance in PQ/HLG non-linearity and BT.2020 gamut is defined as high dynamic range/wide color gamut (HDR/WCG), while that in  $100\text{nit}$  max-luminance and BT.709 gamut is termed standard dynamic range (SDR).

With the proliferation of HDR/WCG display in consumer market, conflicts lies in 2 aspects: Content providers are eager to start HDR/WCG service while such content is still scarce. Also, users are expecting to enjoy better experience via readily-available HDR/WCG display while most service is still in SDR. This entails inverse tone-mapping (ITM) which converts SDR to HDR/WCG. Most AI-ITMs (§2.2) aim at remastering legacy SDR footage, they mainly focus on recovering degradation by end-to-end network, and fail for user-end-display scenario since an edge device (e.g. set-to-box) is with limited computation resources. Thus, a 3D look-up table (LUT) suits precisely, since it pre-calculates all  $\mathbb{R}^3 \rightarrow \mathbb{R}^3$  mapping and replaces runtime computation with caching, indexing and interpolation.

Yet, conventional LUT requires designer's expertise in e.g. color science for a *top-down* design and couldn't embrace the merits of big-data in a *bottom-up* learning. Also, fixed LUT lacks adaptability and is hard to follow cinephotographer's diverse technical/artistic intent between SDR and HDR/WCG in real workflow. Hence, we combine LUT with AI: We train the method with latest refined HDR/WCG dataset [Guo et al. 2023], and endow it with adaptability by merging 5 basic LUTs [Zeng et al. 2020a] using network-generated weights.

While most AI-LUTs (§2.3) are oriented for 8-bit SDR, 10/12-bit HDR/WCG requires larger LUT size, *i.e.* less efficiency, for the same error level [Vandenberg and Andriani 2020]. Therefore, we must utilize LUT's *precision* of sparse representation (packing vertices) more efficiently. One solution is assigning non-uniform packing within single LUT. For example, [Andriani et al. 2021] has denser packing at lower range based on that HDR/WCG's numerical distribution concentrates more on smaller codewords than SDR, while [Yang et al. 2022a] lets packing vertices gather at the range where AI think is with more non-linearity. However, for method's generalization, we can't assume the numerical distribution of SDR and expect the method to interpolate less error only on such SDR.

To this end, we consult traditional ITM *e.g.* [Mohammadi et al. 2020], and use 3 LUTs with distinct contribution on dark, middle and bright luma ranges. For each LUT, its non-uniform packing on SDR's RGB cube (*precision*) is assigned denser vertices on specific range, by Eq.2, so its interpolation result will have less error only on corresponding range. In this case, we use pixel-wise map (Eq.3) to let each result contribute their best range to final result. Also, with the constraint of this map, LUT's output on HDR/WCG's RGB cube (*content*) will also concentrate on their own responsible ranges.

By redistributing the *precision* and *content* of 3 LUTs ( $N=17$ ), we have more efficient utilization than conventional (AI-)LUT ( $N=33$ ), and reach an acceptable result compared to other AI solutions. Experiments are as follows: The first is ablation study on packing vertices (*precision* redistribution), contribution map (guidance of *content* redistribution) and LUT initialization *etc.* The rest are comparative experiments using both HDR/WCG-tailored metrics and subjective experiment *etc.* Our contributions are:

- In the filed of AI (learning-based) ITM, to the best of our knowledge, our method is the first 3D-LUT-based, and currently the fastest under UHD/4K resolution.
- In AI (learning-based) LUT, we make the first attempt adapting higher-bit-depth HDR/WCG, and discuss the impact of some rarely-studied ingredients *e.g.* LUT initialization.

## 2 RELATED WORK

### 2.1 Traditional Inverse Tone-mapping

[Akyüz et al. 2007] use fixed  $\gamma$  curve to expand SDR's luminance to HDR, while [Bist et al. 2017; Masia et al. 2017] add parameter(s) controlled by SDR statistics, and [Luzardo et al. 2018] further improve the shape of  $\gamma$  curve. Some algorithms still apply global expansion, yet use piecewise function based on different perceptual characteristics of bright and dark luminance ranges: [Meylan et al. 2007] use polygonal function, *Method C* in [ITU 2021] set  $58.5\text{nit}$  knee-point and use a 2-piece linear-exponential curve, [Chen et al. 2015] use 2-piece 2-order polynomial with real-time pivot search, while [Mohammadi et al. 2020] apply 3-piece 1-order polynomial expansion directly in PQ non-linear domain.

Rather a numerical different expansion, some methods use spatial extra operator. [Banterle et al. 2007] expand SDR by inverting existing tone-mapping operator [Reinhard et al. 2002] and combining with SDR residual by a weight map, SDR highlight area is then expanded by a guidance map from density estimation. [Rempel et al. 2007] use simpler expansion curve, yet more complicated guidance map by image pyramid, this guidance map is later improved by

[Kovaleski and Oliveira 2009]. [Huo et al. 2014] use Retina-theory-assisted curve affected by not only SDR's global statistics, but also neighboring pixels.

Yet, traditional ITM algorithms: (1) only define an  $\mathbb{R}^1 \rightarrow \mathbb{R}^1$  mapping on luminance, thus chrominance components need to be borrowed/adjusted from SDR to HDR. (2) are incapable recovering degradation. (3) have user-controlled parameters *i.e.* lacked adaptability. (4) will not expand color volume when comes to HDR/WCG, and no advanced WCG pixels will be produced if only color space conversion (CST)[ITU 2015] is appended, rather gamut expansion.

## 2.2 Learning-based (AI) Inverse Tone-mapping

Based on above deficiencies, researchers have turned to AI approach which conduct  $\mathbb{R}^3 \rightarrow \mathbb{R}^3$  mapping directly from SDR to HDR/WCG. Some AI method *e.g.* [Eilertsen et al. 2017] is for image-based lighting, not media industry, so we follow the taxonomy in [Eilertsen et al. 2021; Guo et al. 2023] to call them single-image HDR reconstruction (SI-HDR). Here, a method is termed ITM if its output is claimed in PQ/HLG and BT.2020 gamut.

First, global operations still play an important role in AI: [Kim and Kim 2019; Mustafa et al. 2022] are pixel-independent, while [Chen et al. 2023b,a, 2021; Kim et al. 2023; Shao et al. 2022; Xu et al. 2023] use multi-step network where at least one sub-step belongs to global operation. Meanwhile, [Mustafa et al. 2022; Yao et al. 2023] use reversible operation. Modulation is popular obtaining adaptability in AI-ITM: modulation in [Chen et al. 2021; Xu et al. 2022a, 2023] is broadcast among all pixels, while that of [Chen et al. 2023a; He et al. 2023, 2022; Shao et al. 2022; Xu et al. 2022b] is spatially different. For video application, [Cao et al. 2022; Xu et al. 2022c, 2023, 2022b, 2019b; Zou et al. 2020] improve the temporal coherency processing consecutive frames, [He et al. 2023; Kim et al. 2018, 2019, 2020; Xu et al. 2022c; Yao et al. 2023; Zeng et al. 2020b; Zhang et al. 2023] conduct joint ITM and super-resolution considering HD/UHD resolution discrepancy. [Chen and Shi 2021; Kim and Kim 2019; Tang et al. 2022] utilize traditional ITM as bypass or pre-processing to reduce the workload of AI part. Other motivations include: [Xu et al. 2019a] is for badly-exposed SDR, and [Cheng et al. 2022; Guo et al. 2023] explore the impact of degradation model in training *etc.*

We further conclude their intended **application scenario** in Tab.1. As seen, the majority is designed for front-end remastering.

## 2.3 Learning-based (AI) 3D-LUT

Since above remastering-oriented end-to-end AI methods are too bulky for user-end, we turn to global (pixel-independent) AI operation with better efficiency: [Yan et al. 2016] predicts pixel's polynomial basis function, [Gharbi et al. 2017] learns per-pixel affine transformation coefficient in bilateral space, [Bianco et al. 2020; Guo et al. 2020] estimate channel's global curve independently (no cross-channel contamination). [Hu et al. 2018; Park et al. 2018] predict the decision on an all-global image processing pipeline (ISP), and [He et al. 2020; Wang et al. 2022] use  $1 \times 1$  convolution (no receptive filed). Considering the expressiveness and efficiency of each approach, we finally turn to AI-3D-LUT.

So, we first investigate the status-quo of AI-LUT: Except non-3D LUTs for super-resolution[Jo and Kim 2021; Li et al. 2022; Yin

et al. 2023], medical imaging[Yu et al. 2021] and multi-exposure fusion[Jiang et al. 2023] *etc.*, the rest (Tab.2) are all 3D LUTs of RGB triplet which enable color manipulation. We only describe their ideas and refer to §9 of [Kang 2006] for LUT basics. The first AI 3D LUT[Zeng et al. 2020a] merges 3 basic LUTs to an adaptive one using neural-network-generated weights (basic LUTs are also trainable). Since LUT consists of output's sparse expression (*content*) and its input packing (*precision*), subsequent work lies in 2 aspects:

The first technical route is the expressiveness of LUT *content*: [Wang et al. 2021] merges  $3 \times 10$  basic LUTs to 10 and predict 10-channel pixel-wise category map to guide the weighted sum of 10 look-up result. [Liu et al. 2023] is similar and use network-predicted 'context' (another dimension) map to merge 3 basic 4D LUTs conducting  $\mathbb{R}^4 \rightarrow \mathbb{R}^3$  mapping. [Zhang et al. 2022a] flattens 3D LUTs to 2D images before adaptive multi-layer fusion. Meanwhile, LUT's efficiency is also ameliorated: [Zhang et al. 2022b] finds a compressed representation of 3-D LUT, so they can merge up to 20 basic LUTs with minimum overhead. With this compressed representation, [Chen et al. 2023c] increases the number of basic LUTs to 2048 for stronger adaptability needed in photorealistic style transfer. While [She and Xu 2022] decouples a 3D LUT into several 2D LUTs (respectively on R-G, R-B and G-B channel) with fewer size.

The second idea is on LUT's packing *precision*: [Yang et al. 2022b] applies 3 learned 1D LUTs before 3D look-up, which resembles §9.4 of [Kang 2006] and equals to 3D LUT with non-uniform packing interval. [Yang et al. 2022a] shares similar idea, but different source of non-uniformity: they directly set each vertices interval controllable, similar to [Andriani et al. 2021; Monga and Bala 2010].

## 3 PROPOSED METHOD

### 3.1 Module Design

Given  $\mathbf{x} \in \mathbb{R}^{3 \times h \times w}$  the single frame of input SDR in *gamma* non-linearity and BT.709 RGB primaries (gamut),  $\mathbf{y} \in \mathbb{R}^{3 \times h \times w}$  the output HDR/WCG frame in PQ non-linearity and BT.2020 gamut, our method (Fig.1(c)) can be expressed as below:

$$\mathbf{y} = \sum_{l \in \{b, m, d\}} p_l(\mathbf{x}) \cdot \mathbf{y}_l, \quad \mathbf{y}_l = \text{interp.}(\mathbf{x}, \text{LUT}_l, \mathbf{v}_l) \quad (1)$$

where  $l \in \{b, m, d\}$  represents specific LUT on **b**right, **m**iddle or **d**ark luma range,  $p_l(\mathbf{x}) \in \mathbb{R}^{3 \times h \times w}$  is the per-pixel & per-channel contribution map for the weighted fusion of 3 look-up results  $\mathbf{y}_l$  ( $\mathbf{y}_b, \mathbf{y}_m$  and  $\mathbf{y}_d$ )  $\in \mathbb{R}^{3 \times h \times w}$ , determined by 'luma probability'.

**3.1.1 Precision redistribution.** For each range  $l$ ,  $\text{interp.}(\cdot)$  stands for look-up and trilinear interpolation on  $\mathbf{x}$  using the learned  $\text{LUT}_l$  with packing vertices  $\mathbf{v}_l$ . Keeping the number of vertices along  $[0, 1]$  (*i.e.* LUT size  $N$ ) unchanged, [Andriani et al. 2021; Monga and Bala 2010; Yang et al. 2022a] tell us that conventional vertices can be set to non-uniform, to reach denser representation and consequently less interpolation error in specific range. Therefore, one of our discriminate treatment of 3 luma ranges is that each LUT's  $\mathbf{v}_l$  is designed to have different non-uniformity:

$$\begin{cases} \mathbf{v}_b = \mathbf{v}_u^{1/(1.4+0.8\bar{x})} \\ \mathbf{v}_d = \mathbf{v}_u^{2.2-0.8\bar{x}} \\ \mathbf{v}_m = \frac{3\pi\mathbf{v}_u - \cos(3\pi\mathbf{v}_u) + 1}{3\pi + 2} \end{cases}, \quad \mathbf{v}_u = \text{linspace}(0, 1, N) \quad (2)$$

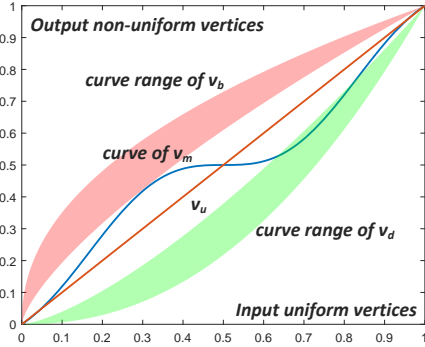
**Table 1: Motivation and application scenario of AI-ITM: most are for front-end remastering, not our user-end display.**

Claimed application scenario	Front-end remastering	Undeclared	User-end display (ours)
Multi-step & global operation	[Chen et al. 2023b,a, 2021; Shao et al. 2022; Xu et al. 2023]	-	[Kim and Kim 2019; Kim et al. 2023; Mustafa et al. 2022]
Using reversible operation	-	-	[Mustafa et al. 2022; Yao et al. 2023]
Using modulation	[Chen et al. 2023a, 2021; Shao et al. 2022; Xu et al. 2022a, 2023, 2022b]	[He et al. 2022]	[He et al. 2023]
Improving temporal coherency	[Xu et al. 2023, 2022b, 2019b; Zou et al. 2020]	[Cao et al. 2022; Xu et al. 2022c]	-
Joint super-resolution	[Kim et al. 2018, 2019, 2020; Zeng et al. 2020b; Zhang et al. 2023]	[Xu et al. 2022c]	[He et al. 2023; Yao et al. 2023]
Combining traditional method	[Chen and Shi 2021; Tang et al. 2022]	-	[Kim and Kim 2019]
Other motivation	[Cheng et al. 2022; Guo et al. 2023; Xu et al. 2019a]	-	-

**Table 2: Status-quo of AI-3D-LUT. We streamline them to 4 ingredients: (1) how the expressiveness of learned LUT(s) is improved, by the number of basic LUTs (#basicLUT, col.2) and introducing extra dimension (extraD, col.4) with certain number of possible values (#) etc., (2) what the neural network is designed to learn (col.5), (3) packing strategy (col.6) and (4) interpolation (col.7).**

AI-LUT methods	Expressiveness of the trained LUT(s)			Output of neural network(s)	Packing intervals (input sampling)	Interpolation
	#basicLUT	LUTsize	extraD (#)			
A3D-LUT[Zeng et al. 2020a]	3×1	3×33 <sup>3</sup>	-	weights (of basicLUTs)	uniform	trilinear
SA-LUT-Nets[Wang et al. 2021]	3×10	3×33 <sup>3</sup>	'category' (10)	weights & category map	uniform	trilinear
4D-LUT[Liu et al. 2023]	3×1	3×33 <sup>4</sup>	'context' (33)	weights & context map	uniform	quadrilinear
CLUT-Net[Zhang et al. 2022b]	20×1	3×5×20	-	weights	uniform	trilinear
NLUT[Chen et al. 2023c]	2048×1	3×32×32	-	weights	uniform	trilinear
F2D-LUTs[She and Xu 2022]	6×3	2×33 <sup>2</sup>	chan. order (3)	weights	uniform	bicubic
DualBLN[Zhang et al. 2022a]	5×1	3×36 <sup>3</sup>	-	LUTs fusion map	uniform	trilinear
AdaInt[Yang et al. 2022a]	3×1	3×33 <sup>3</sup>	-	weights & intervals	learned non-uniform	trilinear
SepLUT[Yang et al. 2022b]	no	3×9/17 <sup>3</sup>	-	directly 1D & 3D LUT	learned pre-nonlinear	trilinear
ITM-LUT (ours)	5×3	3×17 <sup>3</sup>	luma prob. (3)	weights	explicitly-defined non-uniform	trilinear

where  $\bar{x}$  is  $x$ 's arithmetic mean on specific R/G/B channel, it endows  $v_b$  and  $v_d$  with adaptability. As seen, we transfer uniform vertices  $v_u \in \mathbb{R}^{N \times 1}$  to non-uniform  $v_l$  by curves in Eq.2 and Fig.2.

**Figure 2: The non-linear curves (Eq.2) to redistribute uniform vertices (horizontal axis) to non-uniform (vertical axis).**

As in Fig.2, these curves will make  $v_b/v_m/v_d$  respectively denser near  $x=1/0.5/0$ . Meanwhile, since SDR( $x$ )-HDR/WCG( $y$ ) relation is monotonically-increasing, such  $v_b/v_m/v_d$  will also reach more precise result respectively in  $y$ 's higher/middle/lower range.

**3.1.2 Contribution redistribution.** However, specific  $v_l$  will only boost performance in its targeted range, e.g.  $v_d$  has denser representation near  $x$ 's 0 and consequently less error on  $y$ 's lower range, yet sparser near  $x$ 's 1 and worse on  $y$ 's rest higher range. Our solution is making the final result  $y$  a combination of  $y_b/y_m/y_d$ 's own better ranges: As in Eq.1, we use  $x$ 's 'luma probability'  $p_l \in \mathbb{R}^{3 \times h \times w}$

(Fig.6) to determine the per-pixel contribution of  $y_b$ ,  $y_m$  and  $y_d$ :

$$\begin{cases} p_b(x) = \text{clamp}(\frac{x-t_b}{1-t_b}, 0, 1) \\ p_d(x) = \text{clamp}(\frac{x-t_d}{0-t_d}, 0, 1) \\ p_m(x) = 1 - p_b(x) - p_d(x) \end{cases}, x \in [0, 1] \quad (3)$$

where threshold  $t_b=0.55$  &  $t_d=0.45$  controlling each  $y_l$ 's contribution are determined in §4.1(2). For example,  $LUT_d(y_d)$  will not contribute to the higher  $y$  whose contribution should belong to  $LUT_b$ . Note that  $p_b+p_m+p_d=1 \forall x \in [0, 1]$ , so weighted result  $p_l(x) \cdot y_l$  can be directly added ( $\sum$  in Eq.1) without scaling. In this case, e.g. pixel  $x_i=0.3$  is with  $[p_b, p_m, p_d]=[0, 1/3, 2/3]$ , so corresponding  $y_i$  comes in 0, 1/3, 2/3 numerical portion from  $y_b$ ,  $y_m$  and  $y_d$ .

**3.1.3 Content Redistribution.** Till now, we have redistributed the precision of 3  $N=17$  LUTs distinctly to bright, middle and dark ranges (Eq.2), and the contribution redistribution (Eq.3) serves as a consequent compensation of their own precision neglect in the rest range. With AI, their *content* (vertices' corresponding output  $y$ , Fig.1 colored dots) will also be redistributed during training.

As seen, each  $LUT_l$  concentrates on own range. The reason is that under the guidance of contribution map (Eq.3), e.g.  $y_d$  will contribute nothing when  $x_i>0.45$ , so any output value corresponding to  $x_i>0.45$  in  $LUT_d$  will become invalid, thus  $LUT_d$  will be trained to abandon them and concentrate on valid dark range.

**3.1.4 LUT adaptability.** From above we know that any final  $LUT_l$  can have a redistributed *content* with the constraint of Eq.3 and training, the current issue is how final  $LUT_l$  should be generated. One option is [Yang et al. 2022b] who set LUT's  $3 \times N^3$  elements as trainable parameters. The drawback is that once LUT is trained, it becomes fixed and will not alter with  $x$ 's statistics. Hence most AI-ITM (Tab.1) involve  $x$ 's statistics by condition[He et al. 2020], while [Mustafa et al. 2022] is by own latent space.



Mechanisms above will not help LUT. Early attempt of LUT's adaptability is mapping SDR to 1D-LUT using regression[Kadu et al. 2019], and for 3D-LUT, we finally consult [Zeng et al. 2020a]: Each of  $LUT_l$  is merged from 5 basic LUTs ( $LUT_{li}, i \in \{0, 1, 2, 3, 4\}$ ) using the neural-network-generated weights ( $[w_{l0}, \dots, w_{li}]^T$ ):

$$LUT_l = \sum_{i=0}^4 w_{li} LUT_{li}, [w_{l0}, \dots, w_{li}]^T = NetW_l(\mathbf{x}_l) \quad (4)$$

In this case, network (Fig.3) can output varying weights for different  $\mathbf{x}$ , and consequently the  $LUT_l$  will become different. Meanwhile, *content* of 5 basic LUTs are also optimized during training.

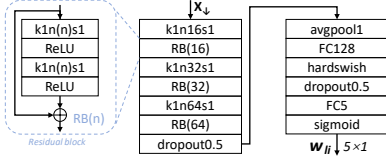


**Figure 3: Structure of weight predictor ( $NetW_l$ ): it consists of lightweight convolution and FC (fully-connected) layers, and is feed with 1/8 down-sampled input  $\mathbf{x}_l$ . Each  $NetW_l$  ( $NetW_b$ ,  $NetW_m$  and  $NetW_d$ ) share the same structure, not parameters.**

## 3.2 Training Strategy

**3.2.1 Initialization.** All weights in  $NetW_l$  are Xavier[Glorot and Bengio 2010] initialized, rest parameters are Kaiming[He et al. 2015] initialized. Note that  $3 \times 5$  basic LUTs [ $LUT_{l0}, \dots, LUT_{l4}$ ] are also trainable, most SDR-oriented AI-LUT (§2.3) initialize them with  $y=x$  and/or  $y=1$ . We show in §4.1.3 that this applies to retouching task whose  $\mathbf{x}$  and  $\mathbf{y}$  are with small numerical discrepancy, yet not ITM whose pixel value alters dramatically due to SDR-HDR/WCG container discrepancy. Therefore, as in Tab.3, we initialize  $LUT_{li}$  with 5 different LUTs which have already been applied in ITM:

**Table 3: Basic LUTs  $LUT_{li}$  are mainly initialized with practical LUTs for ITM (visualized in Fig.8). They consider HDR/WCG discrepancy, and cover different and reasonably large output ranges which will reduce deep leaning's search space.**

basicLUT	initialized with	
$LUT_{l0}$ $l \in \{b, m, d\}$	<b>C_100DW</b>	container conversion from $\gamma(1/0.45)$ SDR to BT.2020 PQ HDR/WCG, w. SDR's defuse white mapped to 100nit, the conversion in most software e.g. macOS Compressor.
$LUT_{l1}$	<b>OCIO2</b>	'sRGB' to 'Rec.2020 ST2084 (1000nits)' conversion provided by OpenColorIO v2.0[Walker et al. 2021].
$LUT_{l2}$	<b>C_203DW</b>	container conversion from $\gamma(1/0.45)$ SDR to BT.2020 PQ HDR/WCG, w. SDR's defuse white mapped to 203nit.
$LUT_{l3}$	<b>DaVinci</b>	'Rec.709/sRGB' to 'Rec.2020/ST2084' conversion provided by grading software DaVinci's 'color space conversion'.
$LUT_{l4}$	<b>identity</b>	LUT recording $y = x$ (identity mapping).

**3.2.2 Loss function.** Given  $\mathbf{x}_p \in \mathbb{R}^{b \times 3 \times 600 \times 600}$  ( $b=4$  is batch size) the  $[0.25x, 1.25x]$  random resized and randomly cropped patch from training set's  $\mathbf{x}$ ,  $\mathbf{y}_p$  the method output and  $\bar{\mathbf{y}}_p$  the GT-HDR counterpart of  $\mathbf{x}_p$ , our loss function can be formulated as:

$$loss = \|\mathbf{y}_p - \bar{\mathbf{y}}_p\|_1 + \sum_l reg_{lut}(LUT_l) \quad (5)$$

where  $reg_{lut} = 0.01 reg_{smooth} + 10 reg_{mono}$ . is 3D-LUT specialized smoothness and monotonicity terms from [Zeng et al. 2020a].

**3.2.3 Training set.** Training set has recently received more attention in ITM[Cheng et al. 2022], we use 3848 HDR/WCG frames from latest-refined HDRTV4K[Guo et al. 2023] dataset as label. However, SDR there contains more degradation simulating legacy SDR, while user-end-received SDR is generally with quality control i.e. less degradation. Also, global operations including LUT are incapable recovering degradation. Therefore, we 'degrade' HDR/WCG to SDR by down-conversion in DaVinci software (rather HDRTV4K's original degradation models) so our input SDR contains less degradation thus  $l_1$  loss will not compensate for unable-to-recover patterns.

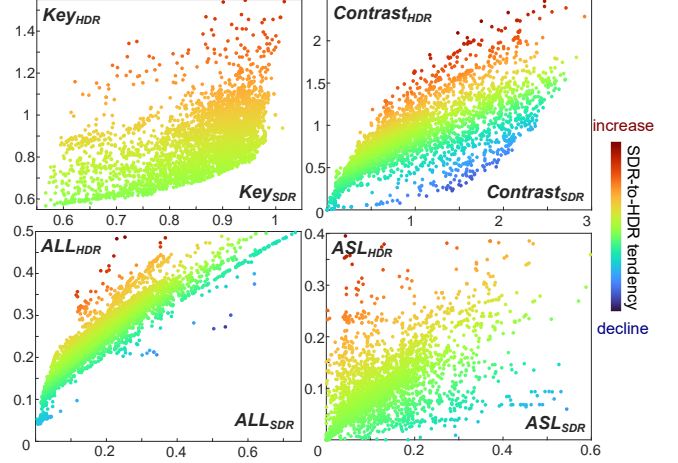


**Figure 4: Training set's diverse SDR-HDR/WCG relationship, each dot is an SDR-HDR/WCG pair: e.g. if SDR-HDR/WCG relation is fixed, dots should be around a single curve, and method will consequently learn a undesired fixed transform.**

Also, the prerequisite for AI to learn adaptability is that it already exists in training set: SDR-HDR/WCG relation should be diverse so method can learn a varying mapping. To this end, when using DaVinci down-conversion, we ask the colorist to use different setting for different HDR/WCG, and this diverse relation is manifested by *key value*[Luzardo et al. 2018], *contrast*[Luzardo et al. 2018], *ALL* (avg. luminance level) and *ASL* (avg. saturation level) of different SDR-HDR/WCG pairs in Fig.4.

**3.2.4 Others.** Each time dataloader is called, UHD SDR-HDR/WCG pairs are randomly resized and cropped to  $600 \times 600$  patches. Method is based on PyTorch, and optimized using AdaM and a decaying learning rate starting from  $2 \times 10^{-4}$ . Training ends when epoch=35.

## 4 EXPERIMENTS

### 4.1 Ablation Studies

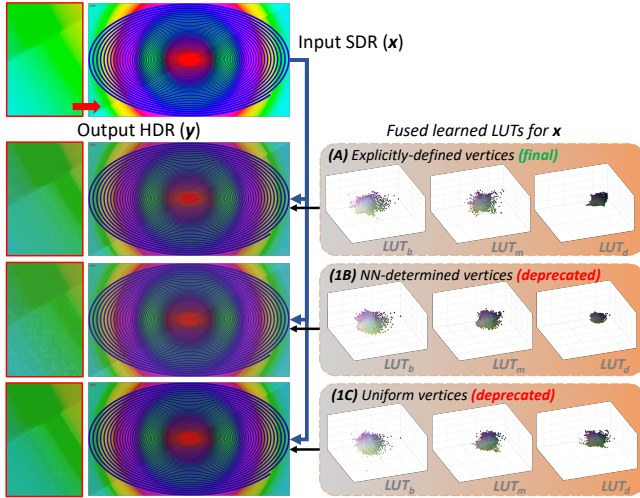
As in Tab.4, we first investigate the impact of 2 core ingredients of our method: non-uniform *precision* redistribution (Eq.2) and contribution map (Eq.3) guiding the redistribution of *content*.

**4.1.1 On non-uniform packing.** The first alternative '1B' keeps vertices non-uniform, yet changes the source of non-uniformity from Eq.2 to 3 neural networks respectively assigned to 3 branches (same structure and initialization as [Yang et al. 2022a]). As seen,

**Table 4: Configurations and quantitative results of ablation studies. \*: Neural network is same as [Yang et al. 2022a].**

Ablations terms		Packing vertices	Luma Probability	LUT initialization	PSNR(dB)	SSIM	$\Delta E$	VDP3
original	A	non-uniform, Eq.2	Eq.3 ( $t_b=0.55, t_d=0.45$ )	5 different LUTs (Tab.3)	34.203	0.9593	17.013	9.0363
§4.1.1: non-uniform vertices	1B	by neural network*			33.883	0.9576	17.316	8.9477
	1C	uniform			34.085	0.9586	17.017	9.0360
§4.1.2: luma probability map (contribution of 3 $y_l$ )	2B	non-uniform, Eq.2	Eq.3 ( $t_b=0.7, t_d=0.3$ )		33.959	0.9575	17.346	9.0015
	2C		Eq.3 ( $t_b=0.9, t_d=0.1$ )		33.986	0.9561	17.572	8.9571
	2D		$p_b=p_m=p_d=1/3$		32.429	0.9516	20.574	8.9435
	2E		further-soft seg. (Eq.6)		33.424	0.9530	18.105	9.0585
	2F		hard seg. ( $t_b=2/3, t_d=1/3$ )		30.938	0.9325	24.200	8.4941
§4.1.3: LUT initialization	3B	Eq.3 ( $t_b=0.55, t_d=0.45$ )	5×C_100DW in Tab.3	33.906	0.9575	16.999	8.9071	
	3C		4×identity + 1×all-1	33.642	0.9582	17.399	8.9906	

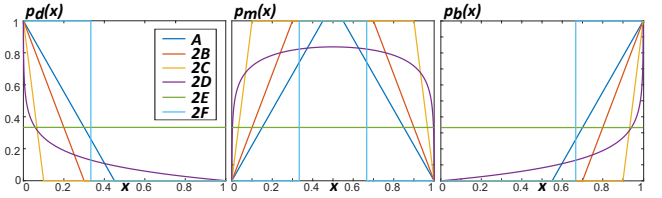
metrics drop more than ‘1C’ (Tab.4) and artifact appears (Fig.5 red box). The reason is that network-determined non-uniformity is hard to follow the assumed emphasis without a proper training constrain, and will thus conflict with the intention of Eq.3, which will be demonstrated in supplementary material. Then, we change vertices back to uniform (1C). In this case, Fig.5 appears a similar visual, yet metrics in Tab.4 drop slightly. In brief, by showing the case of uniform (1C) and conflicting-non-uniform (1B), we prove the effectiveness of non-uniform *precision* redistribution of Eq.2.

**Figure 5: The impact of *precision* redistribution ( $v_l$ , Eq.2): it will affect less the redistribution of  $LUT_l$ 's *content*, yet more on objective metrics in Tab.4.**

**4.1.2 On contribution map.** Here, 4 alternatives are: (1) Changing threshold  $t_b$  and  $t_d$  in Eq.3 *i.e* each branch's contribution: increasing the contribution of  $y_m$  (reducing that of  $y_b$  and  $y_d$ ) slightly (2B) and significantly (2C). (2) Not assigning each  $y_l$  with distinct contribution (2D), this equal to simply stacking the number of basic LUTs. (3) Using soft-curves to determine contribution map (2E):

$$\begin{cases} p_b(x) = 1 - \frac{\log(1+\mu(1-x))}{\log(1+\mu)} \\ p_d(x) = 1 - \frac{\log(1+\mu x)}{\log(1+\mu)} \\ p_m(x) = 1 - p_b(x) - p_d(x) \end{cases}, x \in [0, 1], \mu = 5000 \quad (6)$$

where  $p_b + p_m + p_d = 1 \forall x \in [0, 1]$ , and (4) Hard segmentation where specific pixel  $y_i$  comes from the result of only 1  $LUT_l/y_l$  (2F).

**Figure 6: Luma probability functions  $p_l$  (to generate contribution map from SDR  $x$ ) used in ablation study, A is original.**

All alternative luma probability functions  $p_l(x)$  are illustrated in Fig.6. As in Fig.7, the worst case is 2D whose  $LUT_m$  is even trained to all-0-mapping (disabled). Eq.6 (2E) produces artifact since *e.g.*  $p_d$  there is also responsible for  $y$ 's higher range which it shouldn't be. Also, the primitive way to combine  $y_b$ ,  $y_m$  and  $y_d$  to  $y$  (2F) affects less on the distribution of trained LUT content, yet produces more artifact (Fig.7 red box). Lastly, keeping the shape of original probability curve Eq.3 unchanged, increasing the contribution of  $LUT_m$  slightly (2B) and more significantly (2C) will both affect less on *content* distribution, yet Tab.4 indicate that the contribution of each  $LUT_l$  should be in a reasonable (A&2B) range.

**4.1.3 On LUT initialization.** We then investigate LUT initialization whose particularity is brought by HDR/WCG, and is thus rarely discussed in SDR-oriented AI-LUT (Tab.2). First, in left Fig.8, ‘3B’ initializes basic LUTs with 5 container conversion (C\_100DW in Tab.3). It considers the HDR/WCG-SDR discrepancy, but is less diverse. Then, ‘3C’ follows the same configuration as previous AI-LUT, and neglects the HDR/WCG particularity.

From Fig.8 we know that ‘2B’ affects less on the redistribution of LUT *content* and more on visual artifact (green box), while effect of ‘2C’ is more significant on *content* redistribution and less on artifact. Also, from Tab.4 we know that ‘2C’ drops more than ‘2B’, this indicates that the amount of consideration on HDR/WCG discrepancy is positively correlated with method's performance.

## 4.2 Objective Experiments

**4.2.1 Computation overhead.** For fairness, methods in Tab.5 are all implemented by *PyTorch*, re-trained by same training set, and executed on same *Ubuntu* PC with i7-11700K CPU and A2000 GPU (12GB GRAM). Form Tab.6 col.5-8, single-frame runtime and GRAM consumption on UHD(3840×2160) and HD(1920×1080) resolution we know that: non-I2I(image-to-image, col.9) and global (col.4) AI

**Table 5: The computation overhead of 5 AI-ITM, 3 AI-LUT (both LUT size  $N=33$ ) and 3 AI-retouching methods. As seen, our method best meet the efficiency requirement of user-end display-oriented application.**

Method			Global op. only	UHD resolution		HD resolution		I2I	#net.	#LUT
				runtime	GRAM	runtime	GRAM	network	param.	element
AI-ITM	<b>Deep SR-ITM</b> [Kim et al. 2019]	ICCV'19	×	N/A (GRAM OOM)		1.305s	8099MB	✓	2634k	-
	<b>SR-ITM-GAN</b> [Zeng et al. 2020b]	Access'20	×	2.694s	10539MB	0.608s	5759MB	✓	515k	-
	<b>HDRTVNet</b> [Chen et al. 2021] (ACGM+LE)	ICCV'21	×	2.235s	10165MB	0.559s	5053MB	✓	1404k	-
	<b>FMNet</b> [Xu et al. 2022a]	MM'22	×	2.635s	8715MB	0.697s	5843MB	✓	1302k	-
	<b>LSN</b> [Guo et al. 2023]	CVPR'23	×	1.554s	9639MB	0.406s	3867MB	✓	325k	-
AI-LUT	<b>A3DLUT</b> [Zeng et al. 2020a] ( $N=33$ )	TPAMI'20	✓	0.279s	2483MB	<b>0.051s</b>	<b>2067MB</b>	×	296k	323k
	<b>AdaInt</b> [Yang et al. 2022a] ( $N=33$ )	CVPR'22	✓	0.310s	3015MB	0.060s	2286MB	×	375k	323k
	<b>CLUT-Net</b> [Zhang et al. 2022b] ( $N=33$ )	MM'22	✓	0.907s	<b>2365MB</b>	0.249s	2079MB	×	264k	<b>28k</b>
AI-retouching	<b>NeurSpline</b> [Bianco et al. 2020]	TIP'20	✓	1.087s	3951MB	0.296s	2463MB	×	4457k	-
	<b>DeepLPF</b> [Moran et al. 2020]	CVPR'20	×	1.652s	8038MB	0.401s	3483MB	×	1769k	-
	<b>CSRNet</b> [He et al. 2020]	TPAMI'22	✓	0.958s	10325MB	0.608s	5759MB	✓	<b>35k</b>	-
ours	<b>ITM-LUT</b> ( $3 \times N=17$ )		✓	<b>0.254s</b>	2869MB	0.063s	2145MB	×	452k	221k

**Table 6: Re-trained results of both global and non-global, AI-ITM, AI-LUT and AI-retouching methods. As seen, our method can reach acceptable performance compared with others with sophisticated network.**

Method		Conventional metrics (distance to GT)				Expansion of HDR/WCG volume (%)				Style/aesthetic statistics (%)			
		PSNR(dB)	SSIM	$\Delta E_{itp}$	VDP3	FHLP	EHL	FWGP	EWG	ALL	Contrast	ASL	CF
AI-ITM	<b>Deep SR-ITM</b>	32.804	0.9373	23.570	8.8861	3.5562	0.1558	0.5503	0.1782	20.521	81.345	9.1469	9.6395
	<b>SR-ITM-GAN</b>	32.659	0.9536	20.609	9.0901	2.3079	0.0768	0.5287	0.0799	18.482	80.792	8.5387	9.1991
	<b>HDRTVNet</b>	33.523	0.9562	18.756	9.0964	5.0759	0.5142	0.3354	0.0952	20.798	82.661	9.7860	9.9985
	<b>FMNet</b>	32.938	0.9264	24.405	9.0911	3.8903	0.2969	0.9793	0.1674	20.275	85.030	10.099	9.6456
	<b>LSN</b>	<b>35.617</b>	<b>0.9667</b>	<b>14.666</b>	<b>9.3839</b>	3.7387	0.3885	2.4938	0.1826	19.929	81.453	9.7997	9.9632
AI-LUT	<b>A3DLUT</b>	33.540	0.9539	17.610	8.8209	4.1767	0.4965	0.2151	0.0538	20.293	85.536	9.3331	9.2878
	<b>AdaInt</b>	31.586	0.9378	22.257	8.5561	3.7596	0.4617	0.0666	0.0008	19.864	85.639	9.2363	8.9695
	<b>CLUT-Net</b>	33.511	0.9569	19.363	8.9299	3.8815	0.4780	0.9013	0.2726	20.157	85.457	9.6476	10.441
Fixed LUT ( <b>DaVinci</b> , $N=33$ )		30.042	0.9529	23.996	9.0981	4.4174	0.5429	0.1964	0.0007	21.476	85.172	9.5059	9.2358
AI-retouching	<b>NeurSpline</b>	28.618	0.8545	46.762	8.8730	4.8400	1.3018	3.7184	0.9940	20.894	79.410	12.157	13.906
	<b>DeepLPF</b>	29.774	0.8818	30.977	8.8153	2.5981	0.1581	1.0589	0.0774	19.735	80.675	10.121	10.326
	<b>CSRNet</b>	31.970	0.9283	22.887	9.1484	3.1287	0.2348	0.5777	0.0348	19.493	81.438	9.7322	9.8361
ours	<b>ITM-LUT</b>	34.203	0.9593	17.013	9.0363	4.0031	0.5089	0.6183	0.1897	20.255	85.729	9.4065	9.6538
GT HDR/WCG		-	-	-	-	4.8668	0.7405	2.5877	0.3610	20.749	83.688	9.7584	10.286

methods generally execute faster. Among them, **our method** is the fastest under UHD *i.e.* best for user-end scenario. Note that **CLUT-Net** is the slowest among AI-LUT, since its runtime is mostly spent decompressing its own compressed LUT representation.

**4.2.2 Test set.** We use 400 GT HDR/WCG from HDRTV4K[Guo et al. 2023] benchmark, and corresponding input SDR is ‘degraded’ by *DaVinci* as described earlier. Since SDR is less degraded, conventional metrics (PSNR, SSIM,  $\Delta E_{itp}$  color difference [ITU 2019] and VDP3[Mantiuk et al. 2023]) will less manifest method’s recover ability, but more on adaptability. As in Tab.6, **our method** got acceptable score compared with others with sophisticated network, which means global operation suffice display-end ITM. Also, **our method** surpassed other AI-LUT, which will verify our HDR/WCG-optimized 3-branch LUT design. Note that **AdaInt** underperforms, since its AI-determined non-uniform vertices conflict with HDR/WCG characteristics, as in bottom Fig.9.

**4.2.3 HDR/WCG metrics.** We use fraction/extent of highlight/wide-gamut (pixels) (FHLP/EHL/FWGP/EWG) from [Guo et al. 2023] to measure result’s HDR/WCG volume, and avg. luminance/saturation level (ALL/ASL), contrast[Luzardo et al. 2018] and colorfulness (CF)[Hasler and Suesstrunk 2003] for aesthetics. As seen, when

methods are re-trained, they got similar HDR/WCG metrics. This indicate that the expansion of luminance and color is mostly done by the global  $\mathbb{R}^3 \rightarrow \mathbb{R}^3$  numerical mapping, rather the recovery ability provided by sophisticated network. Overall, as the fastest one, **our method** reached an acceptable expansion of HDR/WCG volume, and a good aesthetic consistency with GT.

**4.2.4 Visuals.** In Fig.9, all methods expand similar color/luminance ( $Y_{xy}$  diagram/waveform). An exception is AI-retouching **NeurSpline** and **DeepLPF** which have no cross-channel contamination, this proves the correctness of deprecating such global operations in ITM. While the rest methods share similar overall-look and high-light/dark detail when HDR/WCG is rendered as SDR.

### 4.3 Subjective Experiments

From Fig.9, we notice that SDR-rendered HDR/WCGs share little difference, yet, it will become significant when displayed on our Canon DP-V3120 HDR/WCG monitor. Therefore, we append a subjective study using this monitor and 10 footage from [ITU 2022]: Each of 10 scenes is displayed as ‘GT-output1-GT-output2...’ in random order, participants (9 total) are asked to rate from 0 to 100 based on how close current output is to GT, and for each rating



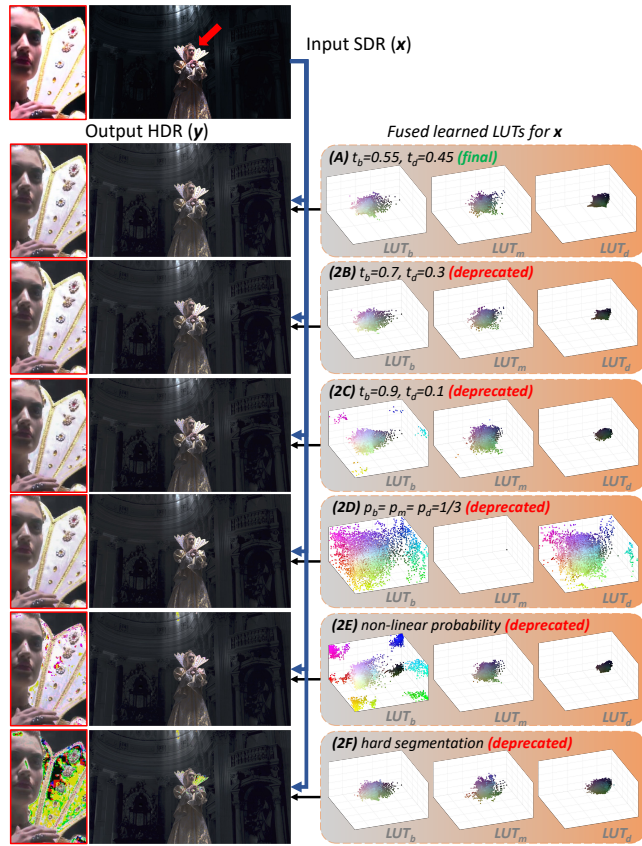


**Figure 7: The effect of contribution redistribution ( $p_i$ , Eq.3): it will mostly change  $LUT_i$ 's learned *content* thus method will map some SDR pixels to undesired color.**

they can optionally select attribution(s) from ‘overall brightness’, ‘local contrast’, ‘hue’, ‘saturation’ and ‘artifact’.

The compared algorithms and GT-to-input degradation are same as objective study. Under such circumstance, **our method** outperforms all other fixed/AI-LUT, and underperforms only 2 of 5 AI-ITM algorithms (Due to space limit, please refer to supplementary material for result). This means our method will suffice user-end application whose SDR is with quality control (less degradation).

## 5 CONCLUSION

This work combined LUT with AI for display-end ITM, and ameliorated it using the bright/middle/dark segmentation inspired by traditional ITM. Our method can: (1) learn a LUT in ‘bottom-up’ manner from any data, (2) execute fast and (3) alter with SDR statistics. Results have demonstrated our edge over AI-ITM, AI/fixed-LUT and AI-retouching methods. Currently the LUT size is 17, and our idea of redistributing *precision* and *content* can be applied to any other common size e.g. 33 or 65, for an efficiency trade-off.

Yet, there are still several aspects calling further study: (1) If there’s a better redistribute of the non-uniformity of 3 smaller LUTs (Eq.2)? (2) Is there a more reasonable contribution map (Eq.3) to cooperate with *precision* redistribution (Eq.2)? (3) Most importantly,

the LUT *content* is currently redistributed by the learning process, is there any way to explicitly define the *content* redistributed, so our idea can be applied outside the learning/AI paradigm? Our method will be more practicable if these concerns are well addressed.

## ACKNOWLEDGMENTS

This work was supported in part by the National Natural Science Foundation of China under Grant 62101290.

## REFERENCES

- Ahmet Oğuz Akyüz, Roland Fleming, Bernhard E Riecke, Erik Reinhard, and Heinrich H Bülthoff. 2007. Do HDR displays support LDR content? A psychophysical evaluation. *ACM Trans. Graph.* 26, 3 (2007), 38–es.
- Stefano Andriani, A Zabot, Giancarlo Calvagno, and JD Vandenberg. 2021. 3D-LUT Optimization for High Dynamic Range and Wide Color Gamut Color Processing. *Electronic Imaging* 2021, 16 (2021), 221–1.
- Francesco Banterle, Patrick Ledda, Kurt Debattista, Alan Chalmers, and Marina Bloj. 2007. A framework for inverse tone mapping. *The Visual Computer* 23 (2007), 467–478.
- Simone Bianco, Claudio Cusano, Flavio Piccoli, and Raimondo Schettini. 2020. Personalized image enhancement using neural spline color transforms. *IEEE Trans. on Image Process.* 29 (2020), 6223–6236.
- Cambridge Bist, Rémi Cozot, Gérard Madec, and Xavier Ducloux. 2017. Tone expansion using lighting style aesthetics. *Computers & Graphics* 62 (2017), 77–86.
- Gaofeng Cao, Fei Zhou, Han Yan, Anjie Wang, and Leidong Fan. 2022. KPN-MFI: A Kernel Prediction Network with Multi-frame Interaction for Video Inverse Tone Mapping. In *Proc. IJCAI*. 806–812.
- Peilin Chen, Wenhan Yang, and Shiqi Wang. 2023b. Revive SDR Videos to HDR Devices: A Learning Paradigm with Hybrid Attention Mechanisms. *IEEE MultiMedia* (2023).
- Qian Chen, Guan-Ming Su, and Peng Yin. 2015. Near constant-time optimal piecewise LDR to HDR inverse tone mapping. In *Digital Photography XI*, Vol. 9404. 187–197.
- Tianyu Chen and Ping Shi. 2021. An Inverse Tone Mapping Algorithm Based on Multi-scale Dual-branch Network. In *2021 International Conference on Culture-oriented Science & Technology (ICCST)*. 187–191.
- Xiangyu Chen, Zheyuan Li, Zhengwen Zhang, Jimmy S Ren, Yihao Liu, Jingwen He, Yu Qiao, Jiantao Zhou, and Chao Dong. 2023a. Towards Efficient SDRTV-to-HDRTV by Learning from Image Formation. *arXiv:2309.04084* (2023).
- Xiangyu Chen, Zhengwen Zhang, Jimmy S Ren, Lynhoo Tian, Yu Qiao, and Chao Dong. 2021. A New Journey From SDRTV to HDRTV. In *Proc. ICCV*. 4500–4509.
- Yaosen Chen, Han Yang, Yuexin Yang, Yuegen Liu, Wei Wang, Xuming Wen, and Chaoping Xie. 2023c. NLUT: Neural-based 3D Lookup Tables for Video Photorealistic Style Transfer. *arXiv:2303.09170* (2023).
- Zhen Cheng, Tao Wang, Yong Li, Fenglong Song, Chang Chen, and Zhiwei Xiong. 2022. Towards Real-World HDRTV Reconstruction: A Data Synthesis-Based Approach. In *Proc. ECCV*. 199–216.
- Gabriel Eilertsen, Saghi Hajisharif, Param Hanji, Apostolia Tsirikoglou, Rafal K Mantiuk, and Jonas Unger. 2021. How to cheat with metrics in single-image HDR reconstruction. In *Proc. ICCV*. 3998–4007.
- Gabriel Eilertsen, Joel Kronander, et al. 2017. HDR image reconstruction from a single exposure using deep CNNs. *ACM Trans. Graph.* 36, 6 (2017), 1–15.
- Michaël Gharbi, Jiawen Chen, Jonathan T Barron, Samuel W Hasinoff, and Frédo Durand. 2017. Deep bilateral learning for real-time image enhancement. *ACM Trans. Graph.* 36, 4 (2017), 1–12.
- Xavier Glorot and Yoshua Bengio. 2010. Understanding the difficulty of training deep feedforward neural networks. In *Proc. 13th international conference on artificial intelligence and statistics*. 249–256.
- Cheng Guo, Leidong Fan, Ziyu Xue, and Xiuhua Jiang. 2023. Learning a Practical SDR-to-HDRTV Up-conversion using New Dataset and Degradation Models. In *Proc. CVPR*. 22231–22241.
- Chunle Guo, Chongyi Li, Jichang Guo, Chen Change Loy, Junhui Hou, Sam Kwong, and Runmin Cong. 2020. Zero-reference deep curve estimation for low-light image enhancement. In *Proc. CVPR*. 1780–1789.
- David Hasler and Sabine E Suesstrunk. 2003. Measuring colorfulness in natural images. In *Human vision and electronic imaging VIII*, Vol. 5007. 87–95.
- Gang He, Shaoyi Long, Li Xu, Chang Wu, Wenxin Yu, and Jinjia Zhou. 2023. Global priors guided modulation network for joint super-resolution and SDRTV-to-HDRTV. *Neurocomputing* 554 (2023), 126590.
- Gang He, Kepeng Xu, Li Xu, Chang Wu, Ming Sun, Xing Wen, and Yu-Wing Tai. 2022. SDRTV-to-HDRTV via Hierarchical Dynamic Context Feature Mapping. In *Proc. ACM MM*. 2890–2898.
- Jingwen He, Yihao Liu, Yu Qiao, and Chao Dong. 2020. Conditional sequential modulation for efficient global image retouching. In *Proc. ECCV*. 679–695.
- Kaiming He, Xiangyu Zhang, Shaoqing Ren, and Jian Sun. 2015. Delving deep into rectifiers: Surpassing human-level performance on imagenet classification. In *Proc.*

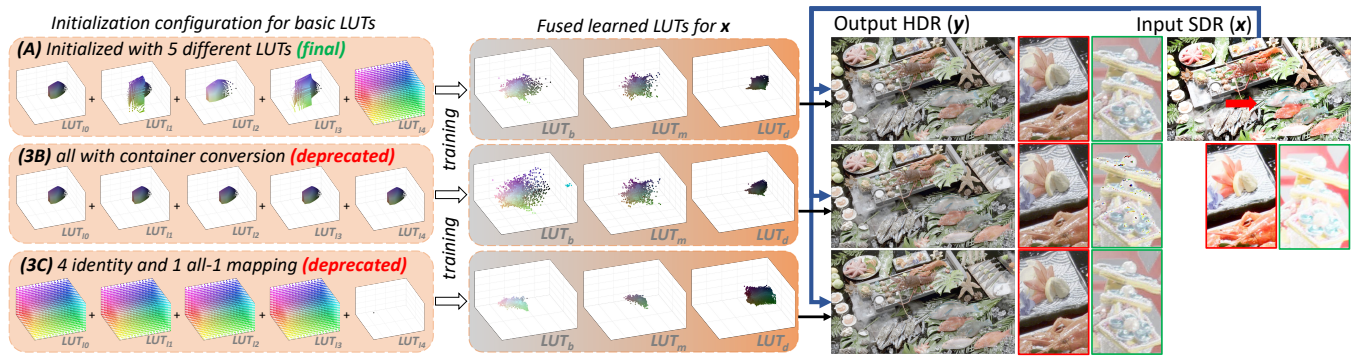


Figure 8: The role of basic LUTs initialization: it will mostly the learn LUT *content* redistribution and produce color artifact if some part of LUT is learned with undeserved mapping. Note that  $LUT_{bi}$ ,  $LUT_{mi}$  and  $LUT_{di}$  ( $i \in \{0, 1, 2, 3, 4\}$ ) are same initialized.

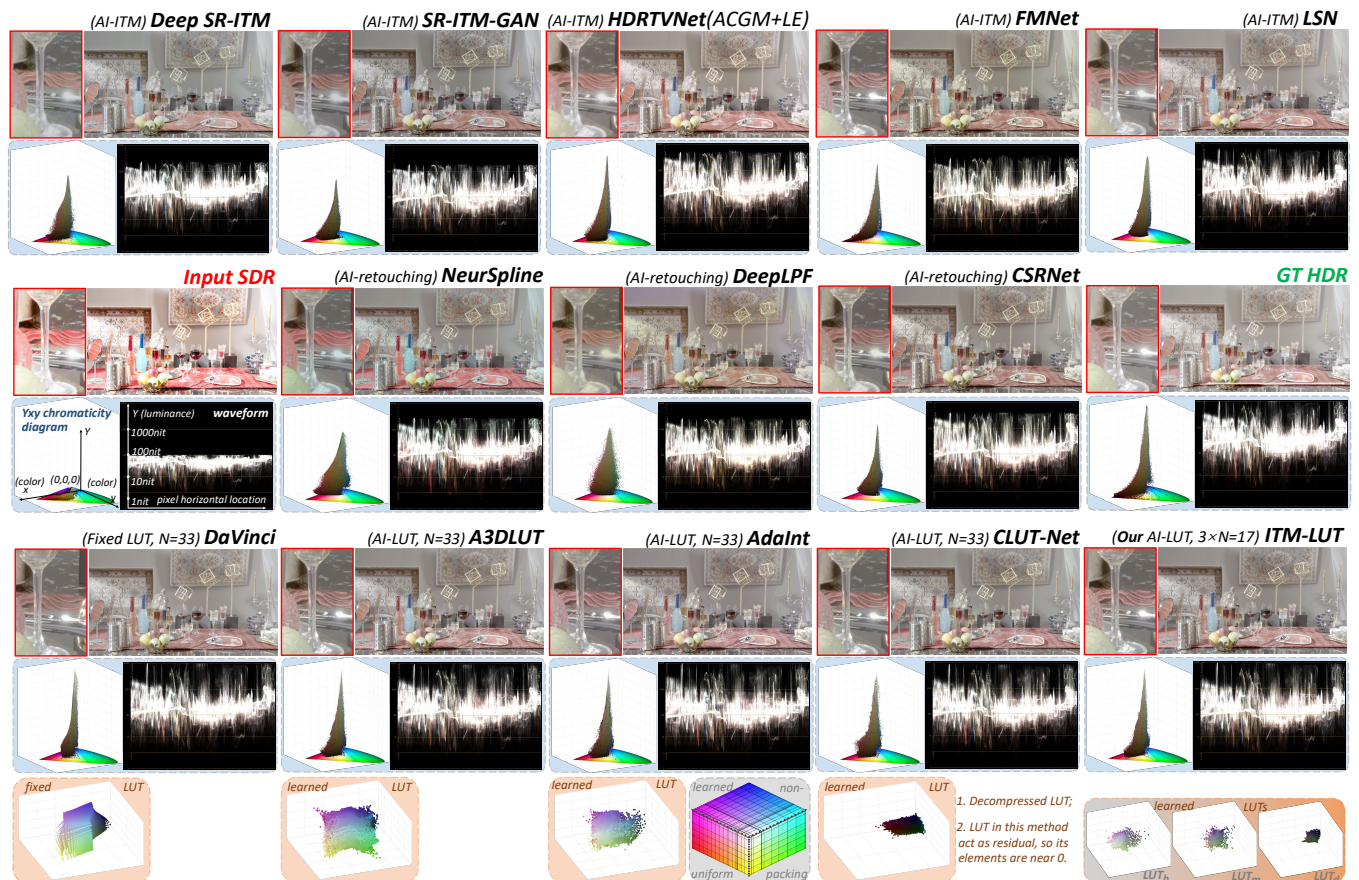


Figure 9: Visual comparison on highlight detail (red box), Xyy chromaticity diagram and waveform (blue box) of both input SDR, result HDR/WCG and GT. Last row are (learned) LUTs of 5 LUT-based algorithms, as seen, they grab the SDR-HDR/WCG relation from training set in different ways. See supplementary material for more.

Yuanming Hu, Hao He, Chenxi Xu, Baoyuan Wang, and Stephen Lin. 2018. Exposure: A white-box photo post-processing framework. *ACM Trans. Graph.* 37, 2 (2018), 1–17.

Yongqing Huo, Fan Yang, Le Dong, and Vincent Brost. 2014. Physiological inverse tone mapping based on retina response. *The Visual Computer* 30 (2014), 507–517.

ITU 2015. *Recommendation ITU-R BT.2087-0: Colour conversion from Recommendation ITU-R BT.709 to Recommendation ITU-R BT.2020* (0 ed.). ITU, Geneva, Switzerland.

ITU 2019. *Recommendation ITU-R BT.2124-0: Objective metric for the assessment of the potential visibility of colour differences in television* (0 ed.). ITU, Geneva, Switzerland.

ITU 2021. *Report ITU-R BT.2446-1: Methods for conversion of high dynamic range content to standard dynamic range content and vice-versa* (1 ed.). ITU, Geneva, Switzerland.



- ITU 2022. *Report ITU-R BT.2245-10: HDTV and UHDTV including HDR-TV test materials for assessment of picture quality* (10 ed.). ITU, Geneva, Switzerland.
- Ting Jiang, Chuan Wang, Xinpeng Li, Ru Li, Haoqiang Fan, and Shuaicheng Liu. 2023. MEFLUT: Unsupervised 1D Lookup Tables for Multi-exposure Image Fusion. *arXiv:2309.11847* (2023).
- Younghyun Jo and Seon Joo Kim. 2021. Practical single-image super-resolution using look-up table. In *Proc. CVPR*. 691–700.
- Harshad Kadu, Neeraj J Gadgil, and Guan-Ming Su. 2019. Reverse tone mapping of high dynamic range video using Gaussian process regression. In *IEEE Conference on Multimedia Information Processing and Retrieval (MIPR)*. 409–414.
- Henry R Kang. 2006. *Computational color technology*. Spie Press Bellingham.
- Dae-Eun Kim and Munchurl Kim. 2019. Learning-based low-complexity reverse tone mapping with linear mapping. *IEEE Trans. Circuits and Sys. for Video Tech.* 30, 2 (2019), 400–414.
- Joonsoo Kim, Kamal Jnawali, and Chenguang Liu. 2023. Efficient-HDRTV: Efficient SDR to HDR Conversion for HDR TV. In *2023 IEEE International Conference on Image Processing (ICIP)*. 1065–1069.
- Soo Ye Kim, Dae-Eun Kim, and Munchurl Kim. 2018. ITM-CNN: Learning the inverse tone mapping from low dynamic range video to high dynamic range displays using convolutional neural networks. In *Proc. ACCV*. 395–409.
- Soo Ye Kim, Jihyong Oh, and Munchurl Kim. 2019. Deep sr-itm: Joint learning of super-resolution and inverse tone-mapping for 4k uhd hdr applications. In *Proc. ICCV*. 3116–3125.
- Soo Ye Kim, Jihyong Oh, and Munchurl Kim. 2020. Jsi-gan: Gan-based joint super-resolution and inverse tone-mapping with pixel-wise task-specific filters for uhd hdr video. In *Proc. AAAI*, Vol. 34. 11287–11295.
- Rafael Pacheco Kovalski and Manuel M Oliveira. 2009. High-quality brightness enhancement functions for real-time reverse tone mapping. *The Visual Computer* 25 (2009), 539–547.
- Jiacheng Li, Chang Chen, Zhen Cheng, and Zhiwei Xiong. 2022. MuLUT: Cooperating Multiple Look-Up Tables for Efficient Image Super-Resolution. In *Proc. ECCV*. 238–256.
- Chengxu Liu, Huan Yang, Jianlong Fu, and Xueming Qian. 2023. 4D LUT: learnable context-aware 4d lookup table for image enhancement. *IEEE Trans. Image Process.* 32 (2023), 4742–4756.
- Gonzalo Luzzardo, Jan Aelterman, Hiep Luong, Wilfried Philips, Daniel Ochoa, and Sven Rousseaux. 2018. Fully-automatic inverse tone mapping preserving the content creator's artistic intentions. In *2018 Picture Coding Symposium (PCS)*. IEEE, 199–203.
- Rafal K Mantiuk, Dounia Hammou, and Param Hanji. 2023. HDR-VDP-3: A multi-metric for predicting image differences, quality and contrast distortions in high dynamic range and regular content. *arXiv:2304.13625* (2023).
- Belen Masia, Ana Serrano, and Diego Gutierrez. 2017. Dynamic range expansion based on image statistics. *Multimedia Tools and Applications* 76 (2017), 631–648.
- Laurence Meylan, Scott Daly, and Sabine Süsstrunk. 2007. Tone mapping for high-dynamic range displays. In *Human Vision and Electronic Imaging XII*, Vol. 6492. 370–381.
- Pedram Mohammadi, Mahsa T Pourazad, and Panos Nasiopoulos. 2020. A perception-based inverse tone mapping operator for high dynamic range video applications. *IEEE Trans. Circuits and Sys. for Video Tech.* 31, 5 (2020), 1711–1723.
- Vishal Monga and Raja Bala. 2010. Algorithms for color look-up-table (LUT) design via joint optimization of node locations and output values. In *Proc. ICASSP*. 998–1001.
- Sean Moran, Pierre Marza, Steven McDonagh, Sarah Parisot, and Gregory Slabaugh. 2020. DeepLpF: Deep local parametric filters for image enhancement. In *Proc. CVPR*. 12826–12835.
- Aamir Mustafa, Param Hanji, and Rafal K Mantiuk. 2022. Distilling Style from Image Pairs for Global Forward and Inverse Tone Mapping. In *The 19th ACM SIGGRAPH European Conference on Visual Media Production (CVMP)*. 1–10.
- Jongchan Park, Joon-Young Lee, Donggeun Yoo, and In So Kweon. 2018. Distort-and-recover: Color enhancement using deep reinforcement learning. In *Proc. CVPR*. 5928–5936.
- Erik Reinhard, Michael Stark, Peter Shirley, and James Ferwerda. 2002. Photographic tone reproduction for digital images. In *Proceedings of the 29th annual conference on Computer graphics and interactive techniques*. 267–276.
- Allan G Rempel, Matthew Trentacoste, Helge Seetzen, H David Young, Wolfgang Heidrich, Lorne Whitehead, and Greg Ward. 2007. Ldr2hdr: on-the-fly reverse tone mapping of legacy video and photographs. *ACM Trans. Graph.* 26, 3 (2007), 39–es.
- Tong Shao, Deming Zhai, Junjun Jiang, and Xianming Liu. 2022. Hybrid Conditional Deep Inverse Tone Mapping. In *Proc. ACM MM*. 1016–1024.
- Dongyu She and Kun Xu. 2022. An Image-to-video Model for Real-Time Video Enhancement. In *Proc. ACM MM*. 1837–1846.
- Rui Tang, Fang Meng, and Lefu Bai. 2022. Zoned Mapping Network from SDR Video to HDR Video. In *2022 IEEE 5th Advanced Information Management, Communicates, Electronic and Automation Control Conference (IMCEC)*. 1466–1472.
- Zhengzhong Tu, Jessie Lin, Yilin Wang, Balu Adsumilli, and Alan C Bovik. 2020. Bband index: a no-reference banding artifact predictor. In *Proc. ICASSP*. 2712–2716.
- JD Vandenberg and Stefano Andriani. 2020. A Review of 3D-LUT Performance in 10-bit and 12-bit HDR BT. 2100 PQ. *SMPTE Motion Imaging Journal* 129, 2 (2020), 59–70.
- Doug Walker, Carol Payne, Patrick Hodoul, and Michael Dolan. 2021. Color management with OpenColorIO V2. In *ACM SIGGRAPH 2021 Courses*. 1–226.
- Tao Wang, Yong Li, Jingyang Peng, Yipeng Ma, Xian Wang, Fenglong Song, and Youliang Yan. 2021. Real-time image enhancer via learnable spatial-aware 3d lookup tables. In *Proc. ICCV*. 2471–2480.
- Yili Wang, Xin Li, Kun Xu, Dongliang He, Qi Zhang, Fu Li, and Errui Ding. 2022. Neural Color Operators for Sequential Image Retouching. In *Proc. ECCV*. 38–55.
- Gang Xu, Qibin Hou, Le Zhang, and Ming-Ming Cheng. 2022a. FMNet: Frequency-Aware Modulation Network for SDR-to-HDR Translation. In *Proc. ACM MM*. 6425–6435.
- Gang Xu, Yuchen Yang, Jun Xu, Liang Wang, Xian-Tong Zhen, and Ming-Ming Cheng. 2022c. Joint Super-Resolution and Inverse Tone-Mapping: A Feature Decomposition Aggregation Network and A New Benchmark. *arXiv:arXiv:2207.03367*
- Kepeng Xu, Gang He, Li Xu, Xingchao Yang, Ming Sun, Yuzhi Wang, Zijia Ma, Haoqiang Fan, and Xing Wen. 2023. Towards Robust SDRTV-to-HDRTV via Dual Inverse Degradation Network. *arXiv:2307.03394* (2023).
- Kepeng Xu, Li Xu, Gang He, Chang Wu, Zijia Ma, Ming Sun, and Yu-Wing Tai. 2022b. SDRTV-to-HDRTV Conversion via Spatial-Temporal Feature Fusion. *arXiv:arXiv:2208.02297*
- Yucheng Xu, Shiyu Ning, Rong Xie, and Li Song. 2019a. GAN based multi-exposure inverse tone mapping. In *Proc. ICIP*. 4365–4369.
- Yucheng Xu, Li Song, Rong Xie, and Wenjun Zhang. 2019b. Deep video inverse tone mapping. In *Proc. bigMM*. 142–147.
- Zhicheng Yan, Hao Zhang, Baoyuan Wang, Sylvain Paris, and Yizhou Yu. 2016. Automatic photo adjustment using deep neural networks. *ACM Trans. Graph.* 35, 2 (2016), 1–15.
- Canqian Yang, Meiguang Jin, Xu Jia, Yi Xu, and Ying Chen. 2022a. AdaInt: Learning Adaptive Intervals for 3D Lookup Tables on Real-time Image Enhancement. In *Proc. CVPR*. 17522–17531.
- Canqian Yang, Meiguang Jin, Yi Xu, Rui Zhang, Ying Chen, and Huaida Liu. 2022b. SepLUT: Separable Image-Adaptive Lookup Tables for Real-Time Image Enhancement. In *Proc. ECCV*. 201–217.
- Mingde Yao, Dongliang He, Xin Li, Zhihong Pan, and Zhiwei Xiong. 2023. Bidirectional Translation Between UHD-HDR and HD-SDR Videos. *IEEE Trans. Multimedia* (2023).
- Guanghao Yin, Xinyang Jiang, Shan Jiang, Zhenhua Han, Ningxin Zheng, Huan Yang, Donglin Bai, Haisheng Tan, Shouqian Sun, Yuqing Yang, et al. 2023. Online Video Streaming Super-Resolution with Adaptive Look-Up Table Fusion. *arXiv:2303.00334* (2023).
- Biting Yu, Luping Zhou, Lei Wang, Wanqi Yang, Ming Yang, Pierrick Bourgeat, and Jurgen Fripp. 2021. SA-LuT-Nets: learning sample-adaptive intensity lookup tables for brain tumor segmentation. *IEEE Trans. Medical Imaging* 40, 5 (2021), 1417–1427.
- Hui Zeng, Jianrui Cai, Lida Li, Zisheng Cao, and Lei Zhang. 2020a. Learning Image-Adaptive 3D Lookup Tables for High Performance Photo Enhancement in Real-Time. *IEEE TPAMI* 44, 4 (2020), 2058–2073.
- Huimin Zeng, Xinliang Zhang, Zhibin Yu, and Yubo Wang. 2020b. SR-ITM-GAN: Learning 4K UHD HDR with a generative adversarial network. *IEEE Access* 8 (2020), 182815–182827.
- Fengyi Zhang, Hui Zeng, Tianjun Zhang, and Lin Zhang. 2022b. CLUT-Net: Learning Adaptively Compressed Representations of 3DLUTs for Lightweight Image Enhancement. In *Proc. ACM MM*. 6493–6501.
- Hengsheng Zhang, Li Song, Wenyao Gan, and Rong Xie. 2023. Multi-scale-based joint super-resolution and inverse tone-mapping with data synthesis for UHD HDR video. *Displays* 79 (2023), 102492.
- Xiang Zhang, Chengzhe Lu, Dawei Yan, Wei Dong, and Qingsen Yan. 2022a. DualBLN: Dual Branch LUT-aware Network for Real-time Image Retouching. In *Proc. ACCV*. 2139–2155.
- Jiaqi Zou, Ke Mei, and Songlin Sun. 2020. Multi-Scale Video Inverse Tone Mapping with Deformable Alignment. In *2020 IEEE International Conference on Visual Communications and Image Processing (VCIP)*. 9–12.